

Geometry-Aware Merge Tree Comparisons for Time-Varying Data with Interleaving Distances

Lin Yan, Talha Bin Masood, Farhan Rasheed, Ingrid Hotz, Bei Wang

Abstract—Merge trees, a type of topological descriptors, serve to identify and summarize the topological characteristics associated with scalar fields. They present a great potential for the analysis and visualization of time-varying data. First, they give compressed and topology-preserving representations of data instances. Second, their comparisons provide a basis for studying the relations among data instances, such as their distributions, clusters, outliers, and periodicities. A number of comparative measures have been developed for merge trees. However, these measures are often computationally expensive since they implicitly consider all possible correspondences between critical points of the merge trees. In this paper, we perform geometry-aware comparisons of merge trees using labeled interleaving distances. The main idea is to decouple the computation of a comparative measure into two steps: a *labeling* step that generates a correspondence between the critical points of two merge trees, and a *comparison* step that computes distances between a pair of labeled merge trees by encoding them as matrices. We show that our approach is general, computationally efficient, and practically useful. Our general framework makes it possible to integrate geometric information of the data domain in the labeling process. At the same time, it reduces the computational complexity since not all possible correspondences have to be considered. We demonstrate via experiments that such geometry-aware merge tree comparisons help to detect *transitions*, *clusters*, and *periodicities* of time-varying datasets, as well as to *diagnose* and *highlight* the topological changes between adjacent data instances.

Index Terms—Merge trees, merge tree metrics, topological data analysis, topology in visualization

1 INTRODUCTION

The efficient analysis of large and complex data is an essential component of a modern scientific workflow. The key ingredients in data analysis are the identification, tracking, and comparison of features expressing essential structures in the data. To this end, *topological data analysis* (TDA) has proven to provide fundamental tools for visual data analysis in terms of abstraction and summarization. Topological descriptors for scalar field data, such as persistence diagrams, barcodes, merge trees, contour trees, Reeb graphs, and Morse–Smale complexes, are among the most widely used applied topological tools in visualization. These descriptors present a great potential for the analysis and visualization of time-varying data. First, they give compressed and topology-preserving representations of data instances. Second, their comparisons provide a basis for studying the relations among data instances, such as their distributions, clusters, outliers, and periodicities; see the work of Yan *et al.* [1] for a recent survey.

In this paper, we are interested in merge trees, which are topological descriptors that record the connectivity among the sublevel sets of scalar fields. Merge trees have seen many applications in science and engineering, including cyclone tracking [2], burning structure analysis [3], and symmetry extraction in materials science [4], [5], to name a few. To employ merge trees for time-varying data or ensembles, a key challenge is to choose an appropriate similarity or distance measure for their comparisons. A number of comparative measures have been developed for merge trees in the literature (see Sect. 2 and [1]), of which many

effectively “forget” about the geometric information from the data domain in the comparative process.

We take a different perspective to utilize merge trees in studying time-varying data, and ask the following question: How can we design a merge tree comparative measure that integrates geometric information from the data domain? We hypothesize that by enriching a merge tree with geometrical information, a comparative measure defined on such enriched merge trees will be sensitive to local or global geometry and thus become beneficial for real-world applications where such geometry is important.

Our work is also motivated by the study of *information content* within a topological descriptor. A few recent efforts have linked information theory with topology. Merelli *et al.* [6] introduced an entropic measure called the *persistence entropy* that captures information within a barcode. Edelsbrunner *et al.* [7] studied TDA in information space by utilizing information-theoretic distances. Recent work by Brown *et al.* [8] posed questions regarding the information content of Reeb graphs, which are topological descriptors closely related to merge trees. Specifically, they asked the following questions: “What information is encoded by a Reeb graph?” “How much information can we recover about the original data from the Reeb graph by solving an inverse problem?” [8]. We are motivated by similar questions regarding the merge tree:

- How much geometric information could we add to a merge tree, so as to increase/enrich its information content, while at the same time improving the comparative process among a pair of “enriched” merge trees in real-world applications?
- Will geometry-aware comparative measures for a set of merge trees improve our understanding of the time-varying data, in terms of its distributions, clusters, and outliers?

We further illustrate the above thought process in Fig. 1. Formally, given a scalar field defined on a connected domain $f_{\mathbb{X}} : \mathbb{X} \rightarrow \mathbb{R}$,

• Lin Yan and Bei Wang are with the University of Utah. E-mails: lynne.h.yan@gmail.com, beiwang@sci.utah.edu.

• Talha Bin Masood, Farhan Rasheed, and Ingrid Hotz are with Linköping University. E-mails: talha.bin.masood@liu.se, farhan.rasheed@liu.se, ingrid.hotz@liu.se.

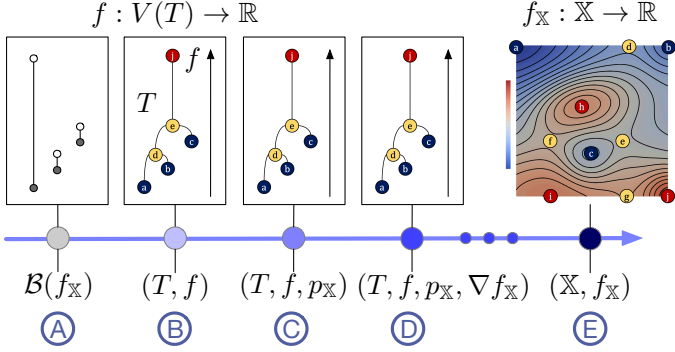


Fig. 1. Given a scalar field $f_X : X \rightarrow \mathbb{R}$, from left to right, we increase the geometric content of the topological descriptors associated with f_X : (A) the barcode of f_X ; (B) the ‘‘classic’’ merge tree (T, f) ; (C) adding the coordinates of critical points p_X of f_X ; (D) adding the gradient information ∇f_X of f_X ; (E) the original scalar field data.

a merge tree records the connectivity of its sublevel sets and is represented as a pair (T, f) , that is, a finite rooted tree T equipped with a function defined on its vertices $f : V(T) \rightarrow \mathbb{R}$; where f is a restriction of f_X to its critical points (see also Sect. 3). As we move from left to right in Fig. 1, we increase the geometric content of a topological descriptor for f_X . We begin with the persistence barcode of f_X in Fig. 1A. By adding slightly more geometric information, that is, how bars in the barcode are glued together, we obtain the ‘‘classic’’ merge tree of f_X , denoted as (T, f) in Fig. 1B. The connection between barcodes and merge trees first appeared (rather implicitly) via the Elder Rule in [9, Page 150], and was further explored in [10], [11], [12]. Although many existing comparative measures on merge trees rely on such a classic definition of merge trees, the focus of this paper is to develop comparative measures on merge trees that encode the geometry of the data domain. Specifically, we focus on enriching a merge tree by encoding the coordinates of critical points p_X of f_X in Fig. 1C. It is also possible to add the gradient information ∇f_X in Fig. 1D. Finally, a merge tree can be enriched with the scalar field f_X itself, possibly rendering the tree redundant in Fig. 1E.

Our objective is to perform geometry-aware comparisons of merge trees. We explore a general notion of merge tree called the *leaf labeled merge tree* [13], [14], which is an abstract tree equipped with a scalar function and a labeling of its leaves. Our main idea is to *decouple* the computation of a comparative metric for a pair of (enriched) merge trees into two steps:

1. A *labeling* step that generates a correspondence between the critical points of two merge trees using various geometric information of the data domain;
2. A *comparison* step that computes distances between pairs of labeled merge trees represented as matrices.

The labeling step makes it possible to integrate geometric information of the data domain, such as the locations of critical points and the gradients of the underlying scalar fields. It also allows the encoding of application-specific domain knowledge. Furthermore, it reduces the computational complexity since not all possible correspondences have to be considered. We provide several heuristic strategies for labeling leaves in a merge tree, namely, *tree mapping*, *Euclidean mapping*, and their *hybrid mapping*. We also discuss a *Morse mapping* strategy based on the gradients of an input scalar field. For the comparison step, we use the *labeled interleaving distance* [13], which encodes the labeling information within matrix representations of merge trees.

Using datasets in scientific simulations, we experimentally evaluate and compare our framework against well-established comparative measures for merge trees, using the bottleneck distance and tree edit distance [15] as the baseline. In summary:

- We provide a general and unifying two-step framework that supports geometry-aware comparisons of merge trees for time-varying data;
- We demonstrate that our proposed framework can help detect *transitions*, *clusters*, and *periodicities* of a time-varying dataset, as well as to *diagnose* and *highlight* the topological changes between adjacent data instances.

Finally, our framework is open source at <https://github.com/tdavislab/MergeTreeMetric>.

2 RELATED WORK

Topological descriptors for scalar fields. A *topological descriptor*, in our context, serves to describe and identify the topological characteristics associated with a data instance (e.g., a scalar field, a vector field, a tensor field, or a multi-field). Most topological descriptors we work with originate from the Morse theory [16]. Well-established topological descriptors for scalar fields include persistence diagrams [17], barcodes [18], merge trees, contour trees [19], Reeb graphs [20] and their discretization, mapper graphs [21], and Morse–Smale complexes [22].

Additional descriptors/visual representations exist that integrate topological *and* geometric information of a scalar field [1]. Correa *et al.* [23] introduced extremum graphs for the design of topological spines, which consist of edges between extrema and shared saddles of scalar fields. Extrema graphs were shown to capture the geometric proximity of the extrema better than the contour trees [23]. Thomas and Natarajan [24] further introduced an augmented extremum graph for geometry-aware symmetry detection in scalar fields. Saikia *et al.* [25] introduced the extended branch decomposition graph, which consists of the branch decompositions of all subtrees of the merge tree. Narayanan *et al.* [26] further introduced a complete extremum graph that associates proximity information for all pairs of extrema.

Merge trees and applications. In this paper, we focus on a type of topological descriptor called merge trees, which track the evolution of the connected components of the sublevel sets of scalar fields. Merge trees have been used to identify and track cyclones [2] and bubbles in Raleigh-Taylor instabilities [27], as well as to analyze burning cells [3] from combustion simulations. Contour trees / merge trees also show up in feature tracking [28], [29], [30], [31].

Merge trees can also be used to study vector and tensor fields. Wang *et al.* [32] used the merge tree to extract robust critical points from vector fields. Wang and Hotz used the merge tree of an anisotropy field to establish the foundation for a stability measure of degenerate points in the tensor field [33]. Jankowai *et al.* [34] utilized such a measure for robust extraction and simplification of 2D tensor field topology.

Topological metrics and kernels. We explore scalar fields by comparing their corresponding topological descriptors, which requires a measure of similarity or dissimilarity between them. The main challenge for the practical use of any similarity measure is its *stability* and *computability*. Recently, existing metrics and kernels for topological descriptors have been investigated extensively [1].

For persistence diagrams, well-established metrics include the bottleneck distance [35], [36] and the Wasserstein distance [37].

They are often used as a comparison baseline for the distance between other types of descriptors (such as merge trees). However, these distances do not incorporate information regarding relations (e.g., nesting) between (sub-)level sets, which are often necessary for analysis [38]. Besides, persistence diagrams do not have the structure of an inner product space (*i.e.* Hilbert space), making it difficult to interface them with machine learning. Instead, several topological kernels have been proposed in the literature [39], [40], making persistence diagrams suitable for learning tasks such as kernel support vector machines.

For Reeb graphs and their variances, namely, merge trees and contour trees, many metrics have been introduced (e.g. [15], [41], [42], [43], [44]). However, many of these metrics remain theoretical and do not have practical implementations. Beketayev *et al.* [38] used the branch decompositions of merge trees to define a distance between them. Their algorithm constructed all possible matchings among pairs of branch decompositions and selected the minimum cost matching among them. Several distances draw inspirations from the Gromov-Hausdorff distance for measuring metric distortion [42], [45]. Bauer *et al.* [42] introduced the functional distortion distance between the Reeb graphs, which was then utilized to compare metric graphs [46]. Sridharamurthy *et al.* [15] introduced an edit distance between merge trees that admits efficient computation. Their edit distance is defined as the minimum cost of a set of restricted edit operations (e.g., delete, insert, and relabel) that transforms one merge tree into another.

Apart from global structural comparison, distance metrics have also been developed based upon local structures. Thomas and Natarajan [4] defined a similarity measure for comparing subtrees of a contour tree and use it to group similar subtrees together to extract symmetric structures in scalar fields. Saikia *et al.* [25] performed structural comparison and extracted repeating topological structures by comparing all subtrees of two merge trees against each other. For hybrid descriptors, Narayanan *et al.* [26] introduced a feature-aware distance metric between extremum graphs that is based on the maximum common subgraph of the complete extremum graphs.

The works of Gasparovic *et al.* [13] and Yan *et al.* [14] are most relevant to the current paper. Gasparovic *et al.* [13] introduced an easily computable metric called the *labeled interleaving distance* that can be used to compare labeled merge trees. Yan *et al.* [14] adapted such a distance in practice for computing average merge trees and visualizing uncertainty. They introduced a few heuristic strategies that generate correspondences between merge trees, which set the foundation for the labeling step in our framework. Compared with [14], we perform a more systematic comparative study on how geometry aware comparative measures for merge trees improve our understanding of time-varying data under various visualization tasks, including the detection of transitions, clusters, and periodicities. We further introduce time-varying pivot tree and dummy vertices strategies, which are shown to be more effective in study the time-varying data, compared with the global pivot tree and dummy leaves strategies first introduced by Yan *et al.* [14].

3 BACKGROUND

In this section, we review the necessary background on scalar field topology surrounding the notions of merge trees, labeled merge trees, and distances between the labeled merge trees.

3.1 Merge Trees and Their Variants

Scalar-field-induced merge trees. Given a scalar field $f : \mathbb{X} \rightarrow \mathbb{R}$ defined on a connected domain \mathbb{X} , a (scalar field induced) merge tree records the connectivity of its sublevel sets. Two points $x, y \in \mathbb{X}$ are considered *equivalent w.r.t. f* , $x \sim y$, if they have the same function value, that is, $f(x) = f(y) = a$, and if they belong to the same connected component of the sublevel set $\mathbb{X}_a := f^{-1}(-\infty, a]$, for some $a \in \mathbb{R}$. A *merge tree* is the quotient space \mathbb{X}/\sim obtained by gluing together points in \mathbb{X} that are equivalent under the relation \sim . Intuitively, it keeps track of the evolution of connected components in \mathbb{X}_a as a increases; see Fig. 2B for an example. Specifically, leaves (*i.e.*, non-root vertices with degree 1) in a merge tree represent the creation of a component at a local minimum, internal vertices (of degree ≥ 3) represent the merging of components, and the root (a degree 1 vertex) represents the entire space as a single component.

Throughout this paper, we denote our *data of interest* as a pair (\mathbb{X}, f) , that is, a connected topological space \mathbb{X} together with a scalar field $f : \mathbb{X} \rightarrow \mathbb{R}$. The quotient space \mathbb{X}/\sim is a new topological space that effectively “forgets” about certain information regarding the data (\mathbb{X}, f) such as the locations of the critical points and the gradient of f .

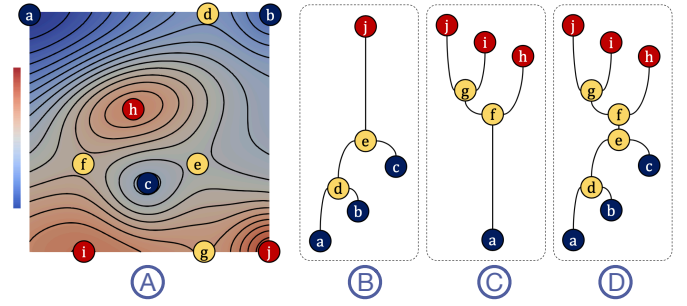


Fig. 2. For the scalar field f in (A): the merge tree of f (*i.e.*, the join tree), the merge tree of $-f$ (*i.e.*, the split tree), and the contour tree of f are illustrated in (B), (C), and (D), respectively.

Labeled merge trees. In this paper, we work with a more general notion of merge trees defined below, which can be considered as an abstract tree coupled with a function f on its vertices, while being oblivious of the possible existence of a scalar field that gives rise to the merge tree.

Definition 3.1. A *merge tree* is a pair (T, f) of a finite rooted tree T with vertex set $V(T)$ and a function $f : V(T) \rightarrow \mathbb{R} \cup \{\infty\}$ such that (i) adjacent vertices do not have equal function value, (ii) every non-root vertex has exactly one neighbor with higher function value, and (iii) the root is the only vertex with the value ∞ [13, Def. 2.1].

Def. 3.1 is closely related to that of *treograms* [47], which is a certain generalization of a dendrogram [48]. Specifically, we focus on the notion of a labeled merge tree. Let $[n]$ denote a set of labels $\{1, 2, \dots, n\}$.

Definition 3.2. A *labeled merge tree*, denoted as a triple $\mathcal{T} = (T, f, \pi)$, consists of a merge tree (T, f) together with a labeling $\pi : [n] \rightarrow V(T)$ that is surjective on the set of leaves [13, Def. 2.2].

π is not required to be injective; thus, a vertex can have multiple labels. π also allows labels for non-leaves by thinking of these as degenerate labeled leaves [13]. For this paper, we work with *leaf-labeled merge trees*, where $L(T) \subset V(T)$ represents its leave set.

Unless otherwise specified, they are referred to as labeled merge trees for the remainder of the paper. We study the space of labeled merge trees that share the *same* label set $[n]$.

Join and split trees. For convenience, we refer to the merge tree of f as the *join tree* and the merge tree of $-f$ as the *split tree* (following the convention in [19]). A join tree (Fig. 2B) tracks the connected component of the sublevel sets of f while a split tree (Fig. 2C) tracks that of the superlevel sets of f . The leaves of a join tree are local minima of f , while the leaves of a split tree are local maxima of f . Combining a join tree and a split tree of f gives rise to its *contour tree* [19] (Fig. 2D), which captures the connectivity among level sets. As illustrated in Sect. 5, studying the join tree or the split tree of time-varying data offers different perspectives on their topological signatures.

Tree and Euclidean distances between vertices. Given an unlabeled merge tree (T, f) , the *intrinsic tree distance* d_t between pairs of vertices is induced by $f : V(T) \rightarrow \mathbb{R}$. For any pair of vertices $x, y \in V(T)$, it is defined as

$$d_t(x, y) = |f(x) - f(lca(x, y))| + |f(y) - f(lca(x, y))|,$$

where $lca(x, y)$ denotes the lowest common ancestor of x and y in T . In other words, $d_t(x, y)$ captures the shortest path between x and y measured by function value differences to their lowest common ancestor.

On the other hand, let $\tau_i : |T^i| \rightarrow \mathbb{R}^2$ denote the geometric embeddings of T_i into the spatial domain (for $i = 1, 2$). The *Euclidean distance* d_e between a pair of vertices $x, y \in V(T)$ is induced by its geometric embedding τ . It is defined as

$$d_e(x, y) = \|\tau(x) - \tau(y)\|_2.$$

3.2 Interleaving Distances Between Merge Trees

A number of metrics may be defined on the space of labeled merge trees. In fact, any metric defined on unlabeled merge trees may be extended to labeled ones by forgetting the label information; which likely turns a metric into a pseudometric [13].

For a labeled merge tree, again let $lca(u, v)$ denote the *lowest common ancestor* of a pair of vertices. We have $lca(u, u) = u$. Let $f(lca(u, v))$ denote its function value.

The *induced matrix* of a labeled merge tree $\mathcal{T} = (T, f, \pi)$, denoted as $M(\mathcal{T}, f, \pi)$, is the matrix $M_{ij} = f(lca(\pi(i), \pi(j)))$ [13, Def. 2.6]. As shown in Fig. 3A-B, the induced matrices of labeled merge trees T^1 and T^2 with a shared label set $[3] := \{1, 2, 3\}$ are defined as follows:

$$M^1 = \begin{bmatrix} 2.0 & 4.7 & 5.2 \\ \cdot & 3.0 & 5.2 \\ \cdot & \cdot & 1.0 \end{bmatrix}, M^2 = \begin{bmatrix} 2.0 & 5.2 & 5.2 \\ \cdot & 3.0 & 4.7 \\ \cdot & \cdot & 1.0 \end{bmatrix}.$$

$M \in \mathbb{R}^{n \times n}$ is symmetric; therefore, it is common to store M as an upper triangular matrix with $n(n+1)/2$ nonzero entries. We use such a convention in our paper. The nonzero terms in M can be linearized into a vector of length $n(n+1)/2$, called the *cophenetic vector* of \mathcal{T} [49], denoted as V .

Turning a labeled merge tree into a matrix (or a vector) enables us to use distances between matrices (or vectors) to obtain distances between trees. We work with the *cophenetic metrics* first introduced by Cardona *et al.* [49] for phylogenetic trees.

Definition 3.3. Given two labeled merge trees $\mathcal{T}^1 = (T_1, f_1, \pi_1)$ and $\mathcal{T}^2 = (T_2, f_2, \pi_2)$ that share the same set of labels $[n]$, the L^∞ -, L^1 -, and L^2 -cophenetic metrics are defined, respectively, as

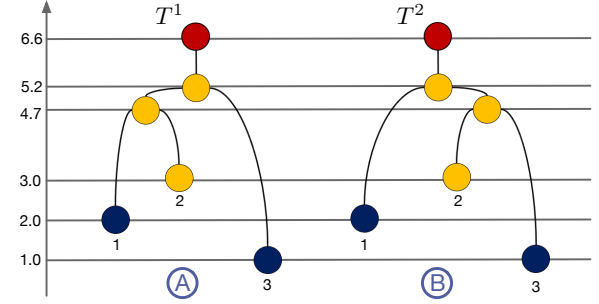


Fig. 3. Labeled merge trees T^1 and T^2 with a shared label set $[3] := \{1, 2, 3\}$.

distances between their corresponding induced matrices M^1 and M^2 [49]:

$$\begin{aligned} d^\infty(\mathcal{T}^1, \mathcal{T}^2) &= \|M^1 - M^2\|_\infty, \\ d^1(\mathcal{T}^1, \mathcal{T}^2) &= \|M^1 - M^2\|_1, \\ d^2(\mathcal{T}^1, \mathcal{T}^2) &= \|M^1 - M^2\|_2. \end{aligned}$$

$\|M\|_\infty$, $\|M\|_1$ and $\|M\|_2$ denote the vector norms, that is, $\|M\|_\infty = \max_{ij} |M_{ij}|$, $\|M\|_1 = \sum_{ij} |M_{ij}|$ and $\|M\|_2 = \sqrt{\sum_{ij} |M_{ij}|^2}$. In other words, the above distances correspond to the L^∞ , L^1 , and L^2 distances between the cophenetic vectors of \mathcal{T}^1 and \mathcal{T}^2 respectively. It is important to point out that d^∞ , d^1 , and d^2 work only on labeled merge trees since we need the (same set of) labels to have a well-defined induced matrix.

d^∞ is also referred to as the *labeled interleaving distance*, denoted as d_I , between a pair of labeled merge trees [13, Def. 2.13] (and subsequently [14, Def. 3.3]), due to its close connection to the interleaving distance of persistence modules [50], [51]. Such a connection is described explicitly in [52]. The interleaving distance of persistence modules has been adapted to merge trees [41], [53], Reeb graphs [54], [55], and Reeb spaces [56], via a category-theoretic perspective [57], [58]. d_I has also been used to compare single-linkage hierarchical clustering [47]. Recent work has established both theoretical [13] and algorithmic [13], [14] foundations for the space of merge trees under the interleaving distances, including computing a form of structural averages for uncertainty visualization [14]. For the remainder of this paper, we work with the interleaving distance d_I with the understanding that $d_I := d^\infty$ for labeled merge trees. For example, as illustrated in Fig. 3, the interleaving distance $d_I(\mathcal{T}^1, \mathcal{T}^2) = \|M^1 - M^2\|_\infty = 0.5$. As illustrated in Sect. 5, one of the main advantages of the labeled interleaving distance d_I is that, as an L^∞ type distance, it helps to diagnose which entries in the induced matrices are likely responsible for the given distance.

3.3 Other Distances

We review a few other distance metrics that are applicable for labeled merge trees. Recall any metric defined on unlabeled merge trees is applicable by ignoring the labeling.

Bottleneck and 1-Wasserstein distance. Given two persistence diagrams X^1, X^2 and a bijection $\eta : X^1 \rightarrow X^2$, the *bottleneck distance* between X^1 and X^2 is defined to be

$$W_\infty(X^1, X^2) = \inf_{\eta : X^1 \rightarrow X^2} \sup_{x \in X^1} \|x \in \eta(x)\|_\infty. \quad (1)$$

The q -Wasserstein distance is

$$W_q(X^1, X^2) = \left[\inf_{\eta: X^1 \rightarrow X^2} \sum_{x \in X^1} \|\eta(x)\|_\infty^q \right]^{1/q}. \quad (2)$$

By definition, W_q becomes W_∞ by setting $q = \infty$. In dimension zero, which is the concern of this paper, there is a correspondence between a merge tree T of f and the persistence diagram X of its sublevel set filtration. Specifically, the branch decomposition of T of f gives rise to the points in the persistence diagram of f . More generally, given a merge tree (T, f) in the sense of Def. 3.1, we could directly define the *persistence diagram of the merge tree*, denoted as X_T , by treating T as a topological space and computing the 0-dimensional persistence of its sublevel set filtration, following a similar construction in [42]. Therefore, we could define the bottleneck distance between the merge trees as the bottleneck distance between the persistence diagrams of the merge trees, that is,

$$d_B(T^1, T^2) = W_\infty(X_T^1, X_T^2). \quad (3)$$

Similarity, we work with 1-Wasserstein distance between the merge trees,

$$d_W(T^1, T^2) = W_1(X_T^1, X_T^2). \quad (4)$$

Edit distance between merge tree. The *edit distance* between merge trees [15] is defined as

$$d_E(T^1, T^2) = \min_S \{\gamma(S)\}, \quad (5)$$

where S is a tree edit operation sequence from T^1 to T^2 that includes edit operations such as “relabel”, “delete”, and “insert”; and γ is a cost function that assigns a non-negative real number to each operation. d_E is an adaptation of and a significant improvement on the constrained unordered tree edit distance [59].

Distance between scalar fields. Finally, given a pair of scalar fields f_1 and f_2 – each sampled at N locations forming a vector of length N , denoted as v_1 and v_2 – we work with Euclidean distances between them in the comparative study, defined as

$$d_F(f_1, f_2) = \|v_1 - v_2\|_2.$$

4 GEOMETRY-AWARE MERGE TREE METRICS

The merge tree metrics described in Sect. 2 are unaware of the geometric information regarding the data domain, such as the locations of the critical points or the gradient of the scalar field. These metrics are defined over the space of *unlabeled merge trees*. To define a geometry-aware metric, we consider a more general space that allows for encoding such information. A suitable space is the space of *labeled merge trees* introduced in Sect. 3. Our two-step framework for merge tree comparisons includes:

1. *Labeling.* This step generates a correspondence between the critical points of two merge trees by encoding the geometric information of the data domain. We describe several labeling strategies – namely, *tree mapping*, *Euclidean mapping*, and *hybrid mapping* – based on topological and geometric information of the scalar fields, respectively.
2. *Comparison.* This step transforms labeled merge trees into their *induced matrices*, and computes distances between labeled merge trees by computing distances between their corresponding induced matrices.

In this section, we describe the labeling step in detail. Suppose we are given a time-varying dataset consisting of l instances of scalar fields defined over a common domain with their corresponding merge trees. There are two requirements to transfer a set of unlabeled merge trees into labeled ones. First, we need to assign a common set of labels between leaves of merge trees, that is, to find leaf correspondences that capture properties of the data domain; see Sect. 4.1. Second, we need to ensure the induced matrices of labeled merge trees are comparable. We introduce *dummy nodes* and *dummy leaves* to the trees to ensure that the resulting induced matrices are of the same size. The latter (dummy leaves) strategy was first introduced in [14]; however, we perform a more systematic study of both strategies in Sect. 4.2. Finally, we introduce the notion of a *time-varying pivot tree*, which is shown to be effective to capture topological transitions in a time-varying setting; see Sect. 4.3.

4.1 Labeling Strategies

Our leaf labeling strategies take as input a pair of unlabeled merge trees T^1 and T^2 that arise from a pair of 2D scalar fields f_1 and f_2 . We consider a tree mapping strategy, a Euclidean mapping strategy, and a hybrid mapping strategy, where the hybrid mapping strategy generalizes the other two strategies.

Given an unlabeled merge tree (T, f) , recall that the intrinsic tree distance between a pair of vertices x and y in the tree is denoted by d_t , and the Euclidean distance between their geometric embeddings is denoted by d_e . d_t and d_e capture the topological and geometric relation between x and y , respectively. To achieve a balance between topology and geometry, we define a hybrid distance as

$$d_h(x, y) = \lambda \cdot d_t + (1 - \lambda) \cdot d_e,$$

for $0 \leq \lambda \leq 1$. d_h generalizes both d_t and d_e . For $\lambda = 1$, $d_h = d_t$ and for $\lambda = 0$, $d_h = d_e$. We thus focus on describing the hybrid mapping strategy, which finds a minimum cost matching between leaves based on their similarities among their d_h distances to other vertices in the tree.

Initial label assignment. Given a pair of unlabeled merge trees T^1 and T^2 , let $V(T^1)$ and $V(T^2)$ denote their respective vertex sets, and $L(T^1)$ and $L(T^2)$ their leaf sets. The goal of an initial label assignment between $L(T^1)$ and $L(T^2)$ is to utilize topology, geometry, or prior knowledge of the data to establish initial correspondences (labels) between subsets of the leaves that share high similarities. These initially matched labels serve as “anchors” during the labeling process, where distances to these anchors are used to assess topological and geometric similarities among the remaining unlabeled leaves.

We use geometric proximities of critical points in the domain under the Euclidean distance as an example. To define a shared label set, the tree with a larger number of leaves is chosen as the *pivot tree* T_p . The leaves of T_p give rise to a *pivot label set*, denoted $S_p := [n]$, where $n = |L(T_p)|$. Let $\pi_p : S_p \rightarrow L(T_p)$ denote a labeling of the pivot tree; *w.l.o.g.*, assume $T_p = T^1$ and π_1 is its leaf labeling. This label set is assigned to $L(T^2)$ via $\pi_2 : S_p \rightarrow L(T^2)$ with a minimum weight matching described below.

To initialize a labeling of $L(T^2)$, we assign a subset of labels in S_p to $L(T^2)$ based on Euclidean distances between $L(T^2)$ and $L(T^1)$ in the embeddings. To do so, we construct a weighted, complete bipartite graph between $L(T^1)$ and $L(T^2)$ where the weight w_{xy} between $x \in L(T^1)$ and $y \in L(T^2)$ is their Euclidean distance in the embedded space constrained by a non-negative threshold ε :

$w_{xy} = d_e(\tau_1(x), \tau_2(y))$ if $d_e(\tau_1(x), \tau_2(y)) \leq \varepsilon$; otherwise $w_{xy} = \infty$. Solving an *assignment* problem of this bipartite graph is to find a matching with a maximum number of edges in which the sum of edge weights is as small as possible, which gives rise to an initial label assignment of leaves in T^2 . In practice, the upper bound ε is chosen based on certain domain knowledge of the data; otherwise $\varepsilon = \infty$ (which is the case for all datasets in Sect. 5).

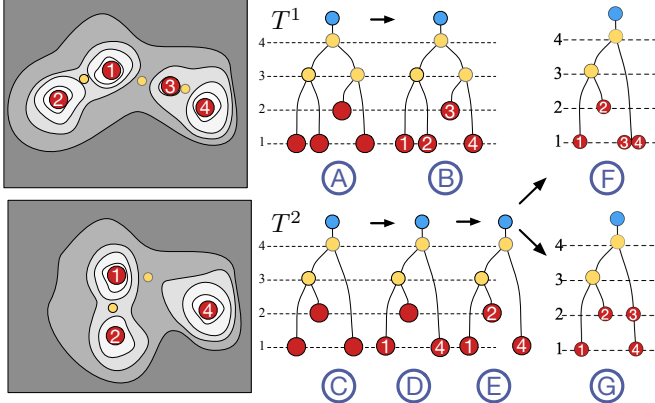


Fig. 4. A labeling of leaves in T^2 (C) against a pivot tree T^1 (A) under the tree mapping strategy, using dummy leaves (F) or dummy vertices (G).

We illustrate this initial label assignment in Fig. 4. We start with a pair of merge trees T^1 and T^2 that arise from a pair of scalar fields. Since $|L(T^1)| = 4 > |L(T^2)| = 3$, T^1 in Fig. 4A is chosen to be the pivot tree, which gives rise to a pivot label set $S_p = \{1, 2, 3, 4\}$, see Fig. 4B. A subset of leaves in T^2 (Fig. 4C) obtains their initial labels $\{1, 4\}$ by solving the above assignment problem (setting $\varepsilon = 0.5$), since the respective leaves are close to one another; see Fig. 4D. Thus, there are two unmatched labels $U_1 = \{2, 3\}$ for T^1 and one unmatched label $U_2 = \{2\}$ for T^2 .

Intermediate label assignment. We now construct a distances matrix D^1 between the unmatched labels and the matched labels in T^1 based on the hybrid distance d_h . A matrix D^2 is constructed similarly. D^1 and D^2 by definition have the same number of columns. We now construct a complete, weighted bipartite graph between the unmatched labels of T^1 and T^2 , where the weight $w_{x,y}$ between a label $x \in U_1$ and a label $y \in U_2$ is given by the L_2 distance between their corresponding rows in D_1 and D_2 , respectively. The final labeling of $L(T^2)$ is obtained by solving another assignment problem in the above bipartite graph.

We continue with the example in Fig. 4. For simplicity, set $\lambda = 1$, d_h is the same as the tree distance d_t . We obtain

$$D_1 = \begin{pmatrix} 4 & 6 \\ 5 & 3 \end{pmatrix}, D_2 = \begin{pmatrix} 3 & 5 \end{pmatrix}.$$

The weight between the label $2 \in U_1$ and label $2 \in U_2$ is $\|(4 \ 6) - (3 \ 5)\|_2 = 2$, and the weight between the label $3 \in U_1$ and label $2 \in U_2$ is $\|(5 \ 3) - (3 \ 5)\|_2 = 8$. By solving the above assignment problem, the unlabeled leaf in T^2 is assigned a label of 2; see Fig. 4E.

4.2 Dummy Leaves and Dummy Vertices

In general, after the intermediate label assignment, there may still be unmatched labels in the pivot tree; for example, the label $\{3\}$ remains unmatched for T^2 in Fig. 4E. The next step is to create dummy labels on T^2 to ensure that it uses the entire pivot label set.

We introduce both *dummy leaves* and *dummy vertices* strategies. The former allows dummy labels only on the leaves, whereas the latter allows dummy labels on the interior of edges.

Dummy leaves. The dummy leaf strategy [14] finds an assignment for each unmatched label in the pivot tree T^1 by duplicating leaves in T^2 . It uses a greedy assignment strategy based on the pairwise distance matrices. The main idea is to find a leaf in T^2 that has the most similar local structure to an unmatched leaf in T^1 . The L_2 distance between the rows from D_1 and D_2 serves as a similarity measure.

Using the example from Fig. 4F, T^1 has an unmatched label 3. The d_t -based pairwise distance matrix between unmatched labels ($\{3\}$) and matched labels in T^1 $\{1, 2, 4\}$ is $D_1 = (5 \ 5 \ 3)$. The d_t based pairwise distance matrix of T^2 encodes distances between leaves $\{1, 2, 4\}$ and matched labels $\{1, 2, 4\}$, forming $D_2 = \begin{pmatrix} 0 & 3 & 6 \\ 3 & 0 & 5 \\ 6 & 5 & 0 \end{pmatrix}$. To find a leaf in T^2 that has the most similar local structure to the unmatched label 3 in T^1 , rows from D_1 and D_2 are compared, which leads to a matching of leaf 3 in T^1 to leaf 4 in T^2 . T^2 now contains one leaf with two labels $\{3, 4\}$, see Fig. 4F.

Dummy vertices. The dummy leaf strategy is well-suited to generate smooth transitions between merge trees [14], but it leads to instabilities in the distance computation. Therefore, we describe a second strategy that adds dummy vertices internal to the branches, which can also be interpreted as adding a branch with zero length. Thus, this strategy ensures that the dummy vertex does not change the tree structure of T^2 . To determine the branch in T^2 where we add a dummy node, a pairwise distance matrix for all candidates is computed and compared to the distances in T^1 .

Let us revisit the example in Fig. 4G. A dummy vertex with a label 3 is added to T^2 with the same scalar value as the leaf 3 of T^1 . This dummy vertex has three candidates, resulting in

$$\text{a pairwise distance matrix } D_2 = \begin{pmatrix} 1 & 2 & 5 \\ 3 & 0 & 5 \\ 5 & 4 & 1 \end{pmatrix}.$$

Compared with $D_1 = (5 \ 5 \ 3)$, the last candidate has the local structure most similar to leaf 3 of T^1 . The result is shown in Fig. 4G, where we add a dummy vertex on the branch of leaf 4 in T^2 .

Induced matrices. After the labeling step, we transform a pair of unlabeled merge trees T^1 and T^2 to a pair of labeled merge trees \mathcal{T}^1 and \mathcal{T}^2 . We can transfer \mathcal{T}^1 and \mathcal{T}^2 to *induced matrices* M^1 and M^2 according to label assignment, as shown in Fig. 4. The pivot label set gives rise to the rows and columns of an induced matrix, as shown below for the example in Fig. 4:

$$M^1 = \begin{pmatrix} 1 & 3 & 4 & 4 \\ & 1 & 4 & 4 \\ & 2 & 3 & & \\ & & 1 & & \end{pmatrix}, M^2 = \begin{pmatrix} 1 & 3 & 4 & 4 \\ & 2 & 4 & 4 \\ & & 1 & 1 \\ & & & 1 \end{pmatrix}.$$

4.3 Time-Varying Pivot Tree

So far we have described strategies to find a leaf-leaf correspondence between a pair of unlabeled merge trees. When moving to a time-varying dataset containing a large number of merge trees, this strategy is, however, not sufficient anymore. It is desirable to have a shared label set for all trees resulting in comparable induced matrices with constant size. Thus, the pivot tree selection plays an important role in our technique and we introduce different ways to approach this problem.

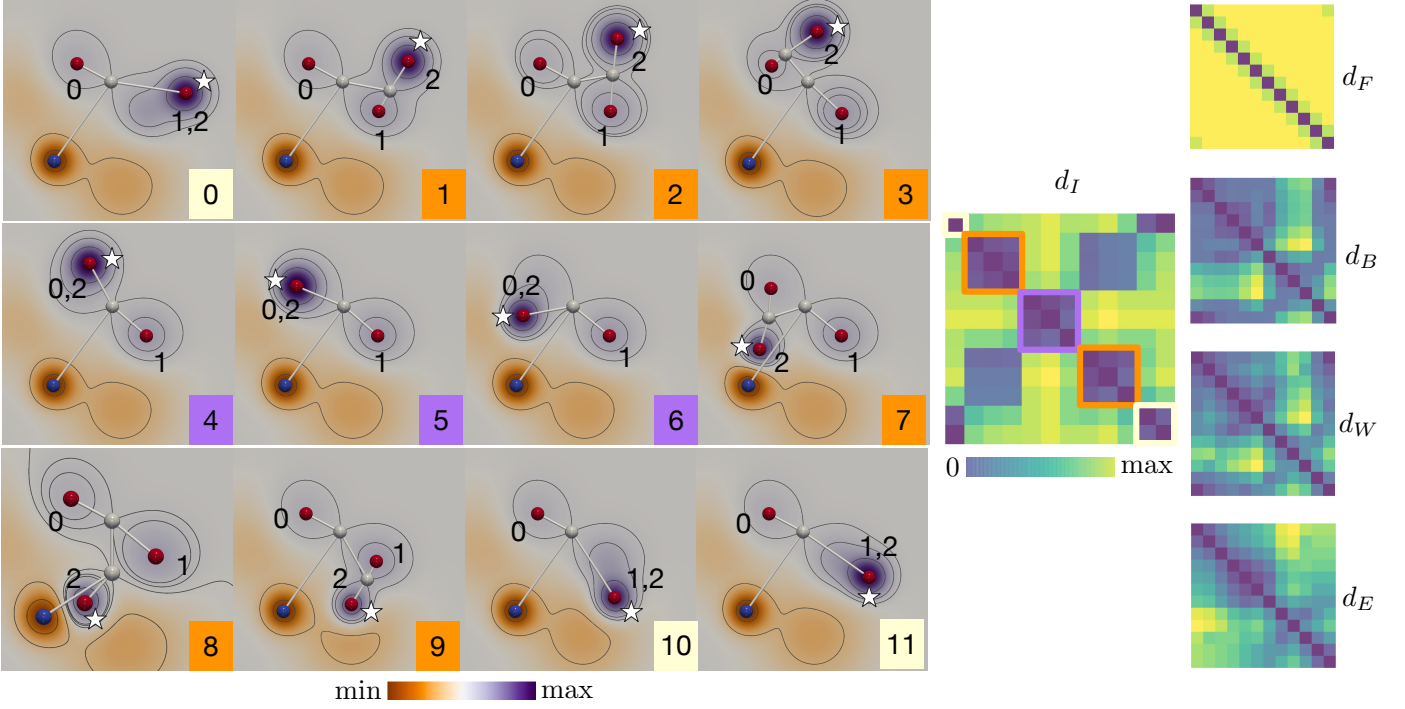


Fig. 5. Moving Gaussian dataset with a hybrid mapping strategy and a time-varying pivot tree. Left: 12 time steps of scalar fields are visualized together with the labeling of the corresponding split trees. Middle and right: distance metrics for d_F , d_B , d_W , d_E , and d_I , respectively, where the zoomed-in version of d_I highlights clusters among the data instances.

Global pivot tree. The first method, first introduced in [14], is a direct extension of the strategy from the matching of two trees described in Sect. 4.1 to many trees. It selects a *global pivot tree* as a tree with the largest number of leaves among all input trees. This tree defines the global label set, and we assign labels to all the other trees using the label set from the *pivot tree*. A major limitation of this approach is the implicit assumption that similarity is a transitive property, which could lead to artifacts for large numbers of trees within a time-varying dataset.

Time-varying pivot tree. To overcome this problem, we introduce a new, *time-varying pivot tree* strategy. The labels are propagated from one tree to the next, capturing temporal changes in a time-varying dataset.

The strategy works as follows: Given a set of merge trees $\{T^0, T^1, \dots, T^l\}$ that arises from a time-varying dataset, let $T_p := T^i$ (for some i) be an initial pivot tree with the largest n number of leaves, thus defining the label set $[n]$. To assign labels to T^{i-1} that immediately precedes T^i , we use T^i as the pivot; thus, T^{i-1} inherits labels from T^i . To assign labels to T^{i-2} , we use T^{i-1} as its pivot instead. In general, T^j will be the pivot tree for T^{j-1} when $j \leq i$, whereas T^j will be the pivot tree for T^{j+1} when $j \geq i$. In a nutshell, the labels are inherited sequentially as we go through the dataset forward and backward from the initial pivot tree in a time-ordered way. Such a strategy works well with time-varying datasets, as demonstrated in Sect. 5.

Pivot-free strategy. The time-varying pivot tree has its advantages and disadvantages. It is desirable for feature tracking within a time-varying dataset, thus supporting the detection of transitions and clusters in real-world datasets; see Sect. 5.1 and Sect. 5.2. However, if the goal is to detect periodicities within time-varying datasets, we will need to effectively “ignore” geometric dependencies among adjacent time instances and treat these instances independently, which leads to an alternative *pivot-free* strategy.

That is, we treat each time instance independently and compute interleaving distances between pairs of instances without requiring a pivot tree or a shared label set across all input trees. In practice, this strategy works reasonably well if we assume the label sets are of roughly the same size; we give an example in Sect. 5.3.

4.4 A Simple Example

We end this section with a simple example involving a synthetic time-varying dataset, referred to as the Moving Gaussian dataset, to illustrate our analysis pipeline. This dataset is generated as a mixture of Gaussian functions centered at seven anchor points in a 2D domain. One of the anchor points (the starred point in Fig. 5A) performs a circular motion in the domain, while the rest remains stationary. This dataset contains 12 time steps modeled as scalar fields. We compute their corresponding split trees and pairwise distance matrices under d_I , d_B , d_W , and d_E , respectively (see Fig. 5B). With the Moving Gaussian dataset, we demonstrate how geometric information coupled with topology helps to reveal its clustering structure, using hybrid mapping, dummy leaves, and time-varying pivot tree strategies. For all our experiments, unless otherwise specified, we set $\lambda = 0.5$ for a hybrid mapping strategy.

Geometric information and a time-varying pivot tree are the two key elements for tracking the moving Gaussian function. As shown in Fig. 5 left (time steps 0 to 11), using a hybrid mapping strategy, our method successfully tracks a moving Gaussian function centered at the starred critical point. This critical point with label 2 performs a counterclockwise circular motion: it merges with local maximum with labels 0 and 1 at time steps 4 and 10, respectively; and splits with them at time steps 7 and 1, respectively. A hybrid mapping considers the geometric positions of critical points in the domain. Therefore, for adjacent instances, stationary critical points are more likely mapped with each other.

Furthermore, as shown in Fig. 5 right, in comparison with other distance metrics (d_F , d_B , d_W , and d_E), the labeled interleaving distance matrix detects three dominant clusters (bounded by purple, orange, and white squares). These clusters are the results of critical points merging and splitting in the time-varying data. In particular, the interactions of the local maximum 2 with other local maxima 0 and 1 at time steps 1, 4, 7, and 10 directly cause the topological transitions of the underlying split trees.

On the other hand, we use a time-varying pivot tree strategy when we give labels to leaves. In this experiment, we pick T^1 as the initial pivot tree since T^1 has the largest number of leaves. Then T^0 and T^2 inherit labels from T^1 . After that, T^2 becomes the pivot tree for T^3 , and T^3 will inherit labels from T^2 and become the pivot tree for T^4 , and so forth. If T^p is the initial pivot tree, T^i will be pivot tree for T^{i+1} when $i \geq p$, whereas T^i will be the pivot tree for T^{i-1} when $i \leq p$. The benefit of using the time-varying pivot tree is that such a labeling strategy can propagate both geometric and topological information corresponding to temporal changes. If we used a global pivot tree strategy from [14], T^1 is the only pivot tree, and current labeling results will change, especially when time instances are far from the global pivot tree temporally. For example, labeling T^7 and T^8 using T^1 as a pivot tree will be different with the current labeling result, no matter which mapping strategy we choose.

5 EXPERIMENTAL RESULTS

In this section, we demonstrate via experiments that geometry-aware merge tree comparisons based on the interleaving distance help to detect *transitions*, *clusters*, and *periodicities* of a time-varying dataset, as well as to *diagnose* and *highlight* the topological changes between adjacent instances.

5.1 Detect and Diagnose Structural Transitions

We demonstrate our method in detecting structural transitions using two flow datasets, namely, the Corner Flow and Heated Flow datasets.

Corner Flow dataset. We first demonstrate our method using the 2D Cylinder Flow Around Corners dataset¹, which we refer to as the Corner Flow dataset. This dataset arises from the simulation of a viscous 2D flow around two cylinders [60], [61]. The channel into which the fluid is injected is bounded by solid walls. A vortex street is initially formed at the lower left corner, which then evolves around the two corners of the bounding walls. We generate a set of split trees from the vertical component of the velocity vector fields based on 94 time instances – they correspond to steps 801-894 from the original 1500 time steps. These instances describe the formation of a one-sided vortex street on the upper right corner; see Fig. 6 left that visualizes the scalar fields associated with time steps 53, 54, 67, and 68.

To separate signals from noise, we apply persistence simplification [17] to the split trees of all instances with a persistence threshold of 0.2. In particular, to guide the selection of the persistence threshold, we employ a set of *persistence graphs*, each of which represent the number of persistence pairs as a function of persistence [62]. The shape of the persistence graph, in particular, a plateau, indicates a stable range of scales to separate noise from signals in the persistence graph [63], [64]. We demonstrate such a simplification process in Fig. 8, where time instance 54 is

shown before and after persistence simplification; the persistence threshold is chosen approximately due to the variabilities across time instances.

Our framework analyzes structural transitions via the pairwise distance matrices. For this experiment, we use hybrid mapping, dummy vertex, and time-varying pivot tree strategies. As shown in Fig. 6 middle, our framework using the interleaving distance d_I captures two obvious structural transitions among adjacent instances, 53 → 54 and 67 → 68. There appear to be clear block structures within the d_I matrix, where the above transitions are highlighted by arrows at the corners of these blocks.

Under the diagnostic setting, we locate critical points in the domain that are responsible for the d_I distance between adjacent instances. A close inspection of this time-varying dataset then reveals that from step 53 to 54, a pair of critical points x and y (enclosed by orange spheres) disappears. Similarly, from step 67 to 68, another pair of critical points u and v (enclosed by orange spheres) disappears. Therefore, d_I highlights structural transitions in the time-varying data, whereas in comparison, only the bottleneck distance d_B is able to capture the same 53 → 54 transition in its matrix representation (Fig. 6 white arrow in d_B).

Heated Flow dataset. We give another example using a 2D Heated Cylinder with Boussinesq Approximation dataset¹, denoted as the Heated Flow dataset. This dataset comes from the simulation of a 2D flow generated by a heated cylinder using the Boussinesq approximation [61], [65]. It shows a time-varying turbulent plume containing numerous small vortices.

We convert each time instance of the flow into a scalar field using the magnitude of the velocity vector. We then generate a set of split trees from these scalar fields based on 300 time steps – they correspond to steps 1000-1299 from the original 2000 time steps. This dataset captures the evolution of small vortices over time. We use hybrid mapping, dummy vertex, and time-varying pivot tree strategies, and apply simplification with a persistence threshold of 0.06.

The results are shown in Fig. 7. We observe two visible structural transitions based on d_I between steps 51 → 52 and 153 → 154 (pointed by white and orange arrows, respectively). Under the diagnostic setting, the structural transition 51 → 52 is caused by the disappearance of a pair of critical points x and y at step 51 (highlighted by green bubbles). The transition 153 → 154 is a result of the disappearance of the pair u and v at step 153.

Two additional structural transitions are detected at 74 → 75, and 75 → 76, as indicated by yellow arrow in the d_I matrix of Fig. 7. However, a closer inspection indicates that such a transition is, in fact, an artifact as a result of persistence simplification, which leads to structural changes of the simplified split trees. We will discuss such artifacts further in Sect. 6.

5.2 Detect Clusters

Our method using the interleaving distance helps to cluster time instances based on their structural differences. We demonstrate the utility of the method using 2D simulations of the Red Sea and a dataset generated from Gerris flow solver.

Red Sea dataset. The Red Sea dataset originates from the IEEE Scientific Visualization Contest 2020², and is generated using a high-resolution MITgcm (Massachusetts Institute of Technology general circulation model), together with remote sensing satellite

1. <https://cgl.ethz.ch/research/visualization/data.php>

2. <https://kaust-vislab.github.io/SciVis2020/>

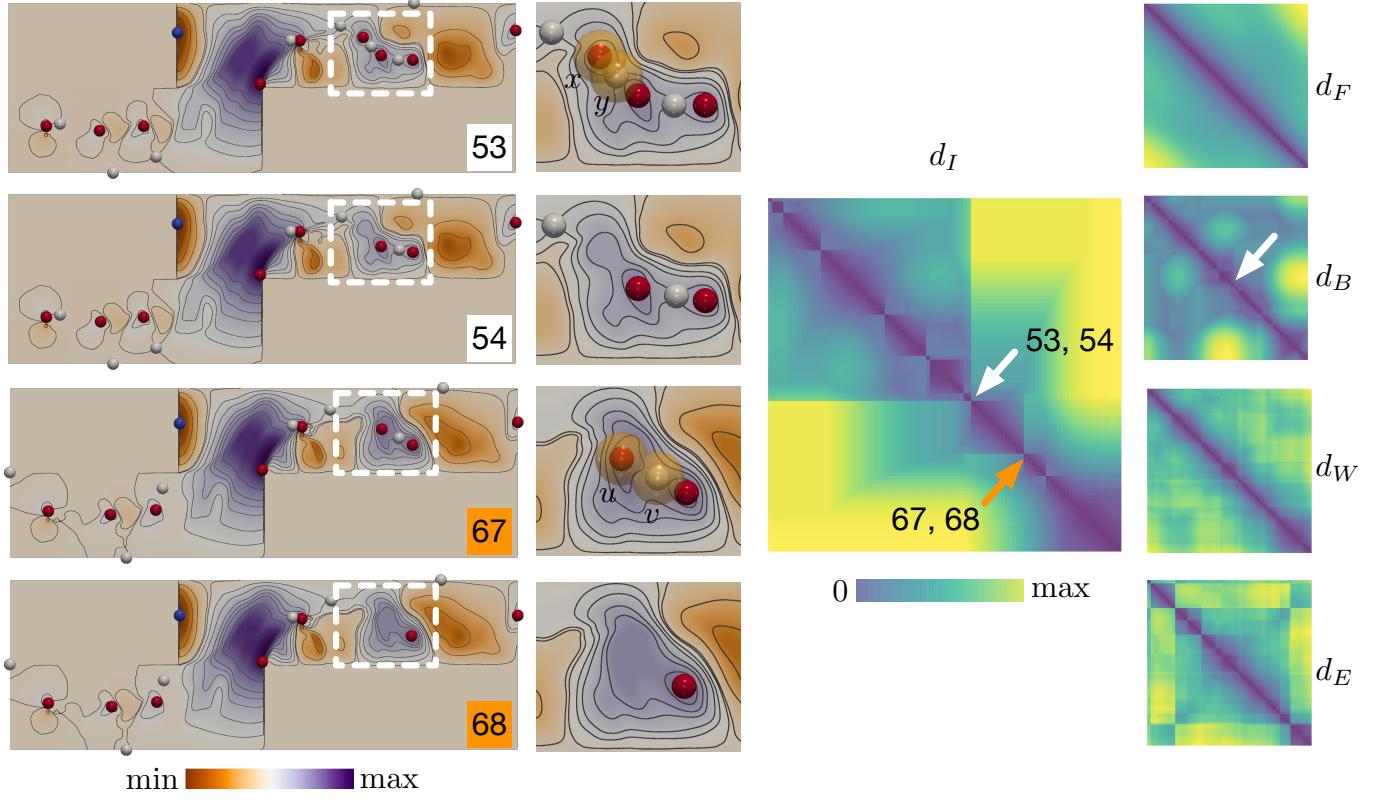


Fig. 6. Geometry-aware merge tree comparisons for a time-varying Corner Flow dataset. Using interleaving distances d_I , our framework helps to diagnose and highlight topological changes between adjacent time steps, in particular, between instances 53 and 54 and instances 67 and 68.

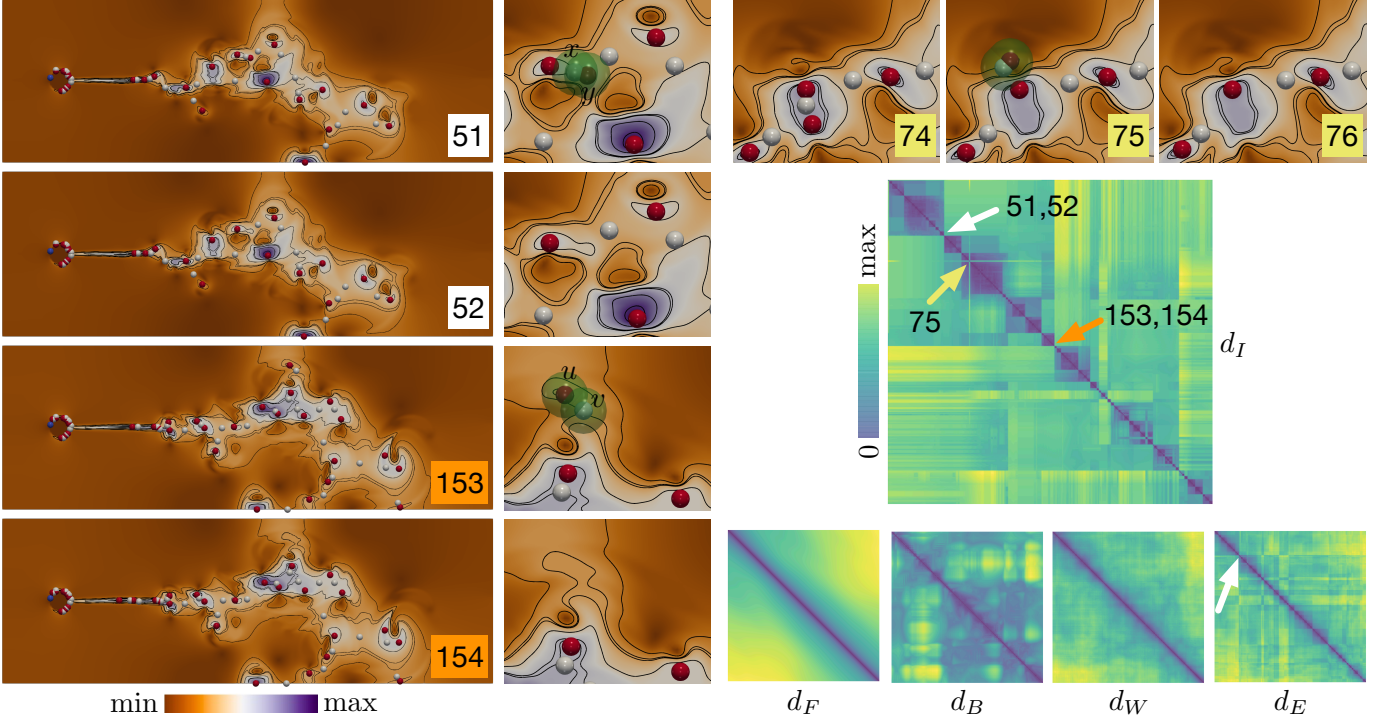


Fig. 7. Heated Flow dataset: geometry-aware merge tree comparisons. Left two columns: selected scalar fields with their zoomed-in views, where local minimum are in blue, saddles are in white, local maximum are in red. Right two columns: pairwise distance matrices for d_F , d_B , d_W , d_E , and d_I , respectively. Arrows in d_I highlight detected structural transitions.

observations. It is used to study the circulation dynamics and eddy activities of the Red Sea (see [66], [67], [68]). For the experiment,

we use the velocity magnitude fields of a particular dataset (named *001.tgz*) with 60 time steps. We generate split trees from the 2D

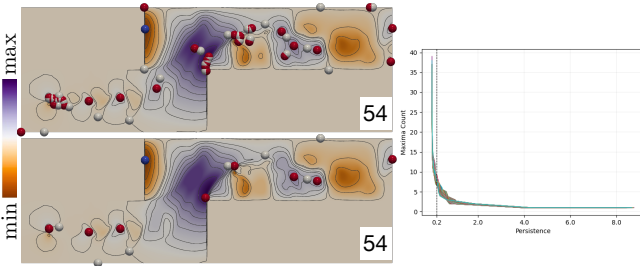


Fig. 8. Corner Flow dataset. Left: time instance 54 before (top) and after (bottom) persistence simplification. Right: a set of persistence graphs used to guide the simplification process.

slices perpendicular to the z-axis ($z = 1$). For this experiment, we use hybrid mapping, dummy vertex, and time-varying pivot tree strategies.

As shown in Fig. 9, the d_I distance matrix clearly indicates four clusters of data instances. It shows that the scalar fields share similar structures from instances 0-6 (in orange square), 10-27 (in white square), 28-54 (in red square), and 55-59 (in magenta square). We visualize several selected scalar fields in Fig. 9 left.

Taking a closer look at their corresponding split trees in Fig. 10, each cluster of data instances share a similar tree structure, especially for some instances in the red cluster (e.g., see instances 40, 45, and 50). In this experiment, d_B and d_W also show some clustering patterns; however, in comparison, d_I offers clearer and more informative clustering pattern.

Wing dataset. The Wing dataset is generated using the software *Gerris flow solver*³. We use its demo flow simulation example involving the “starting vortex”, which is a vortex that forms in the fluid near the trailing edge of an aerofoil (wing) as it is accelerated from rest in a fluid. For our simulation, we set the angle of the aerofoil with respect to the fluid as 20° and generate 40 time steps. The scalar field of interest is the velocity magnitude.

For this experiment, we use hybrid mapping, dummy vertex, and time-varying pivot tree strategies. As shown in Fig. 11, we compute various distance matrices based on the split trees computed for the velocity magnitude field. All the trees are simplified at a simplification threshold of 0.13.

As shown in Fig. 11, the d_I matrix clearly detects five clusters of data instances. The MDS projection of all data instances using d_I further highlights the clustering structures among the scalar fields at different time steps. Whereas d_B , d_W , and d_E also capture some clustering structures in this time-varying dataset, d_I gives rise to clusters that appear to be more separable and visually differentiable. Moreover, based on inspection of the velocity magnitude fields shown in Fig. 11, it is apparent that the five clusters separate the time steps into clusters with similar vortex structures. For example, the major change between the orange and green clusters is the appearance of a strong vortex on the top of the wing in the green cluster. Similarly, notice the two strong vortices in the time steps corresponding to the purple cluster. As one of those vortices exits the domain in the subsequent time steps, the instances are grouped into a different cluster marked as red.

5.3 Detect Periodicities

Finally, we demonstrate our framework in detecting periodicities using the classic 2D von Kármán vortex street dataset, which

we refer to as the VortexStreet dataset. We consider the region of vortex shedding behind the cylinder, and use the velocity magnitude field for comparison as used earlier by Sridharanurthy *et al.* [15].

We use hybrid mapping, dummy vertices, and pivot-free strategies. As shown in Fig. 12, using either the join or split tree, d_B , d_W , and d_E all show a periodicity of length 37. The interleaving distance, d_I , captures the same length of periodicity using the join tree. However, using the split tree, we detect a periodicity of length 75 using d_I . Such a longer periodicity coincides with the periodicity detected using d_F . This periodicity can be justified where both d_I and d_F consider more geometric information in the domain, in comparison with other metrics.

Furthermore, as shown in Fig. 12 left, the positions of local maxima (red points) change more drastically every 37 time steps, in comparison with the positions of local minima (blue points). This finer difference is captured by the split tree version of d_I ; where neither d_B , d_W , nor d_E capture this difference in the behavior of the local extrema.

In this experiment, as mentioned in Sect. 4, a pivot-free mapping strategy works better than a time-varying pivot tree strategy in detecting periodicities.

6 CONCLUSION AND DISCUSSION

In this paper, we introduce a systematic way to integrate geometric information for comparing merge trees. Given a pair of merge trees that arise from scalar fields, our main idea is to decouple the computation of a distance measure into two steps: a labeling step that generates a correspondence between critical points of the merge trees, and a distance computation step that computes the labeled interleaving distance between a pair of labeled merge trees by encoding them as matrices. To encode geometric information, we introduce a hybrid strategy during the labeling step that considers the intrinsic tree distances between critical points and/or the Euclidean distances between their locations in the data domain. We demonstrate that our approach can be used to detect clusters, structural transitions, and periodicity in a way that is either comparable or complementary to existing approaches. There are many directions for future research.

Improved efficiency and robustness. Naively computing the labeled interleaving distance d_I requires access to all entries in the reduced matrix, which takes $O(n^2)$ time. Look into a more scalable computation would be interesting, possibly taking inspiration from the work of Kerber *et al.* [69].

In addition, the labeled interleaving distance coupled with various labeling strategies has strengths and weaknesses. The strategy is shown to detect periodicity that is more sensitive to the underlying geometry, and it enjoys a certain amount of robustness due to its stability properties. However, at the same time, it is not as robust as some other metrics when the underlying data contain a large amount of noise and a large number of features; improving its robustness is left for future work.

Integration of domain knowledge. Our two-step comparative process opens doors to the integration of domain knowledge. The labeling process can be easily extended to not only integrate geometric information from the data domain but also to encode information from its underlying applications. In particular, domain knowledge will be useful during the initial label assignment described in Sect. 4.1.

3. <http://gfs.sourceforge.net/>

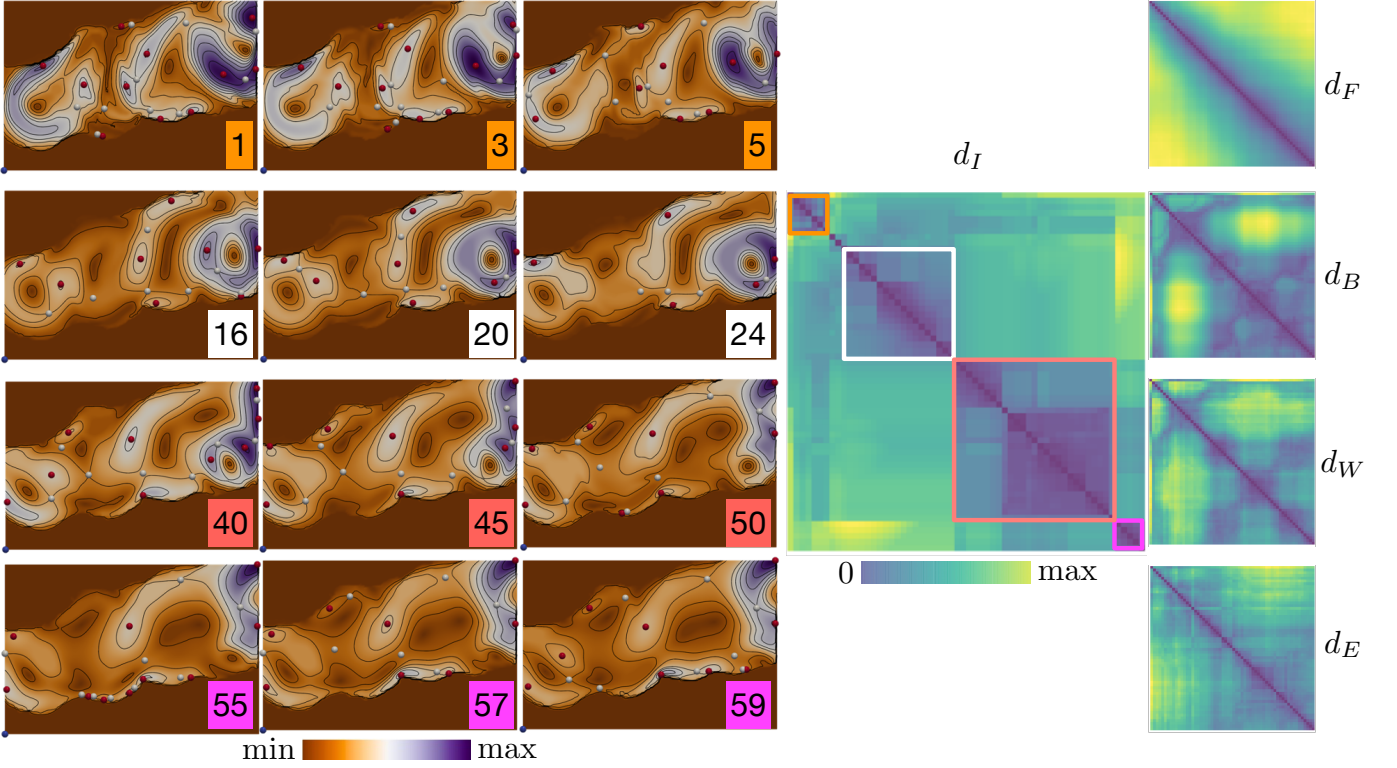


Fig. 9. Red Sea dataset: detect clusters. Left three columns: selected scalar fields drawn from each of the four clusters. Right two columns: pairwise distance matrices for d_F , d_B , d_W , d_E , and d_I , respectively. Colored boxes in d_I highlight the four detected clusters.

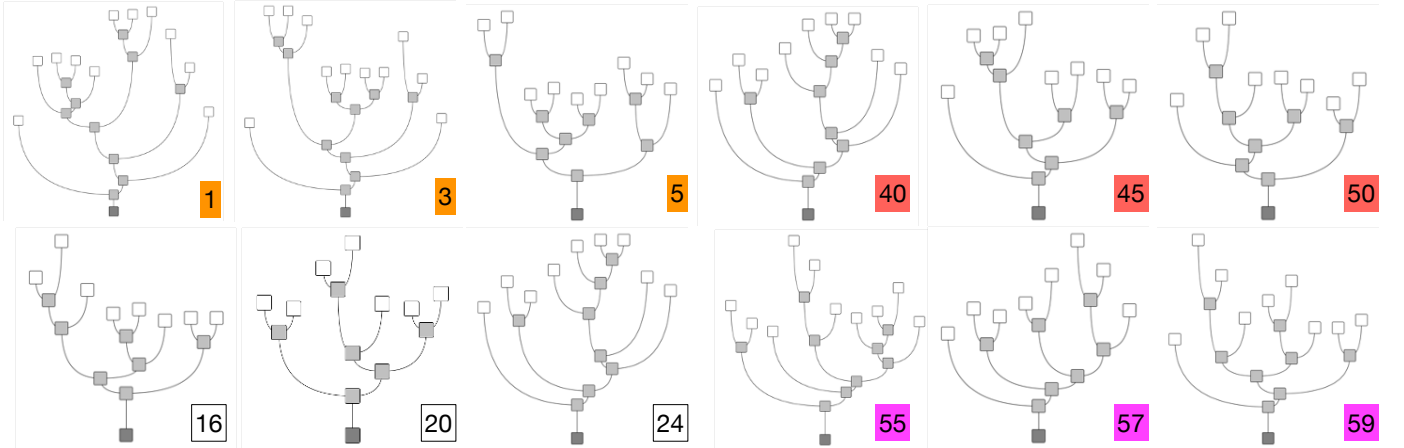


Fig. 10. Red Sea dataset: abstract split trees for selected time steps, cf. Fig. 9.

Other geometry-based labeling strategies. The hybrid labeling strategy based on the tree distance and/or the Euclidean distance between critical points is just one example among many possible geometry-aware labeling strategies. For example, we could adapt a strategy called the *Morse mapping* that has been used for the tracking of critical points [28]. Given a pair of merge trees T^1 and T^2 , the Morse mapping strategy facilitates the gradient flow derived from the scalar fields to define a forward $T^1 \rightarrow T^2$ and a backward $T^2 \rightarrow T^1$ mapping. The forward and backward assignment builds on the partition of the domain provided by the Morse complex [70], which represents the gradient behavior of the scalar field of the data domain. See Fig. 13 for an example of a Morse complex of a 2D scalar field.

Let ∇f denote the gradient of a Morse function $f : \mathbb{X} \rightarrow \mathbb{R}$. An *integral line* at a regular point is a maximal path whose tangent vectors agree with the gradient [70]. The function increases along an integral line, which begins and ends at critical points. The *stable manifold* (or *unstable manifold*) surrounding a critical point x includes x itself and all regular points whose integral lines end (or originate) at x [9, Chap. VI, page 131]. The stable and unstable manifolds of x are denoted as $S(x)$ and $U(x)$, respectively. To define the Morse mapping strategy, we use the unstable manifolds surrounding the local minima of the scalar field (Fig. 13b), which correspond to leaves in the merge tree.

Suppose we are given a pair of merge trees T^1 and T^2 that arise from a pair of scalar fields. Let $x \in V(T^1)$ and $x' \in V(T^2)$ denote

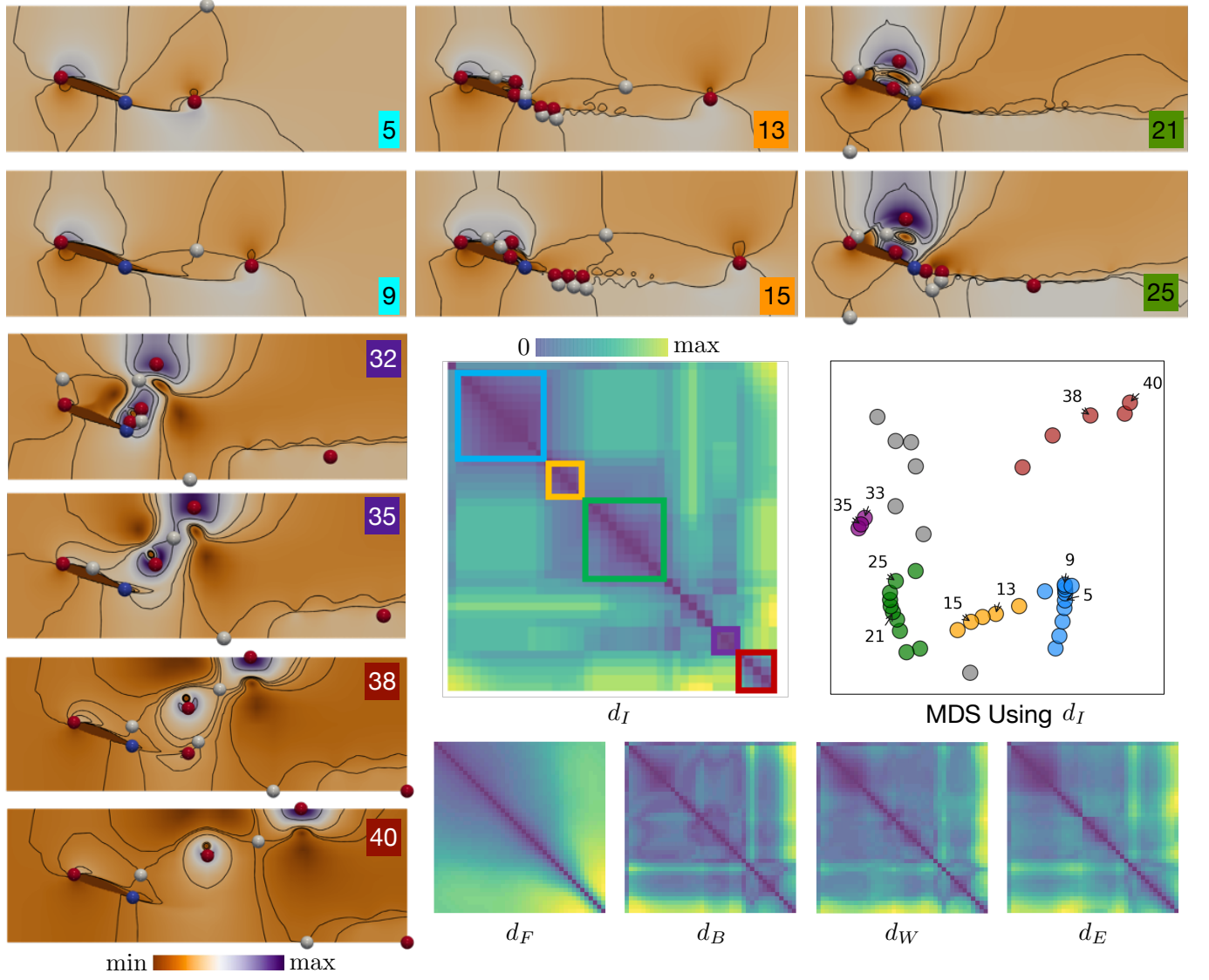


Fig. 11. Wing dataset: detect clusters. Left column and top two rows: selected scalar fields drawn from each of the five clusters. Right column and third row: MDS projection of all the time steps using the d_I metric. Res: pairwise distance matrices for d_F , d_B , d_W , d_E , and d_I , respectively. Colored boxes in d_I highlight the five detected clusters.

a pair of leaves (local minima of the underlying scalar fields). Let $U(x)$, $U(x')$ denote their respective unstable manifolds. We say x is *forward mapped* to x' if $x \in U(x')$ and x' is *backward mapped* to x if $x' \in U(x)$, denoted as $x \rightarrow x'$ and $x \leftarrow x'$, respectively. In other words, we check to which unstable manifold a leave belongs to determine the label assignment. As illustrated in Fig. 14E-F, given a pair of merge trees T^1 and T^2 (Fig. 14A-B) that arise from scalar fields (Fig. 14C-D), local minimum x of T^1 is forward mapped to z' since $x \in U(z')$, whereas z' is backward mapped to x since $z' \in U(x)$.

This strategy leads to three categories of matched leaf pairs: *double connected pairs*, which result in a joint label; and *forward* and *backward connected pairs*, which generate a novel label and introduce a dummy node in one of the trees. For example, x and z' forms a double connected pair in Fig. 14.

Finally, Fig. 14 further illustrates that different mapping strategies between two merge trees result in different label assignments. In this example, merge trees T^1 and T^2 arise from two synthetic 2D scalar fields generated as mixtures of Gaussians. T^1 (Fig. 14A)

contains three leaves that correspond to local minima x, y, z in the domain (Fig. 14C). T^2 (Fig. 14B) contains three leaves that correspond to local minima x', y', z' (Fig. 14C). Using the tree mapping strategy, we obtain a bijective mapping $x \leftrightarrow x'$, $y \leftrightarrow y'$, and $z \leftrightarrow z'$ (cf., Fig. 14A-B). Using the Euclidean mapping strategy, we obtain a different bijective mapping, $x \leftrightarrow y'$, $y \leftrightarrow z'$, and $z \leftrightarrow x'$ (cf., Fig. 14C-D). Finally, using the Morse mapping, we obtain sets of forward ($x \rightarrow z'$, $y \rightarrow y'$, and $z \rightarrow x'$, Fig. 14F) and backward ($x \leftarrow z'$, $y \leftarrow y'$, and $z \leftarrow x'$, Fig. 14E) mappings, forming double connected pairs. Understanding such differences is important in choosing the appropriate strategies for particular datasets, which remains an open question.

ACKNOWLEDGMENTS

This project was partially supported by NSF IIS 1910733 and DOE DE-SC0021015.

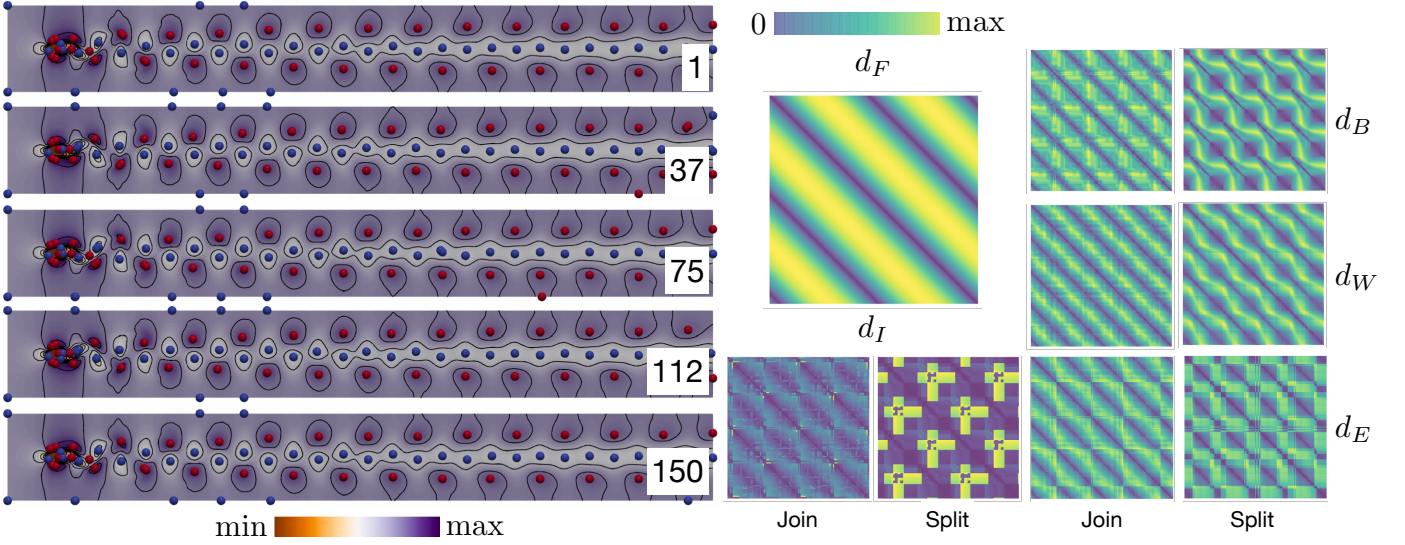


Fig. 12. VortexStreet dataset. Left: five selected time steps are shown for the dataset; notice that the scalar field is mirrored after 37 steps and goes back to the original after 75 time steps. Middle: distance matrices for d_F and d_I , respectively; Right: distance matrices for d_B , d_W , and d_E , using both join and split trees, respectively.

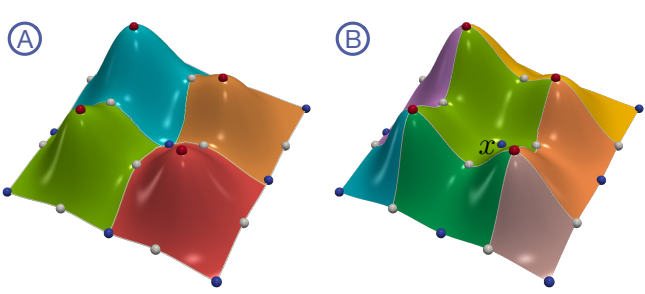


Fig. 13. Given the 2D function f . (a) shows the stable manifolds forming the Morse complex of f . (b) shows the unstable manifolds forming the Morse complex of $-f$; the green cell surrounding the critical point p is an unstable manifold of p .

REFERENCES

- [1] L. Yan, T. B. Masood, R. Sridharamurthy, F. Rasheed, V. Natarajan, I. Hotz, and B. Wang, “Scalar field comparison with topological descriptors: Properties and applications for scientific visualization,” *Computer Graphics Forum*, accepted, 2021.
- [2] A. A. Valsangkar, J. M. Monteiro, V. Narayanan, I. Hotz, and V. Natarajan, “An exploratory framework for cyclone identification and tracking,” *IEEE Transaction on Visualization and Computer Graphics*, vol. 25, no. 3, pp. 1460–1473, 2018.
- [3] P.-T. Bremer, G. Weber, J. Tierny, V. Pascucci, M. Day, and J. Bell, “Interactive exploration and analysis of large scale simulations using topology-based data segmentation,” *IEEE Transactions on Visualization and Computer Graphics*, vol. 17, no. 9, pp. 1307–1324, 2011.
- [4] D. M. Thomas and V. Natarajan, “Symmetry in scalar field topology,” *IEEE Transactions on Visualization and Computer Graphics*, vol. 17, no. 12, pp. 2035–2044, 2011.
- [5] T. B. Masood, D. M. Thomas, and V. Natarajan, “Scalar field visualization via extraction of symmetric structures,” *The Visual Computer*, vol. 29, no. 6–8, pp. 761–771, 2013.
- [6] E. Merelli, M. Rucco, P. Sloot, and L. Tesei, “Topological characterization of complex systems: Using persistent entropy,” *Entropy*, vol. 17, pp. 6872–6892, 2015.
- [7] H. Edelsbrunner, Z. Virk, and H. Wagner, “Topological data analysis in information space,” in *35th International Symposium on Computational Geometry*, ser. Leibniz International Proceedings in Informatics (LIPIcs), G. Barequet and Y. Wang, Eds., vol. 129. Dagstuhl, Germany: Schloss Dagstuhl–Leibniz-Zentrum fuer Informatik, 2019, pp. 31:1–31:14.
- [8] A. Brown, O. Bobrowski, E. Munch, and B. Wang, “Probabilistic convergence and stability of random mapper graphs,” *Journal of Applied and Computational Topology*, in revision, 2020.
- [9] H. Edelsbrunner and J. Harer, *Computational Topology: An Introduction*.

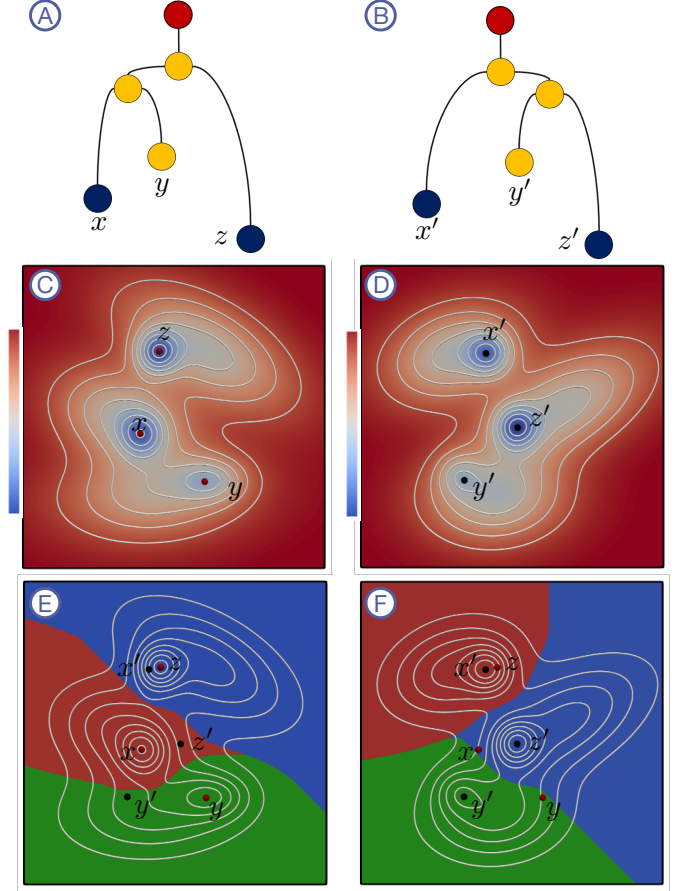


Fig. 14. Comparing three mapping strategies with two synthetic datasets generated as mixtures of Gaussians. Label assignments obtained via tree mapping, Euclidean mapping, and Morse mapping strategies give rise to different labels.

- American Mathematical Society, 2010.
- [10] J. Curry, "The fiber of the persistence map for functions on the interval," *Journal of Applied and Computational Topology*, vol. 2, no. 3-4, pp. 301–321, 2018.
- [11] M. J. Catanzaro, J. M. Curry, B. T. Fasy, J. Lazovskis, G. Malen, H. Riess, B. Wang, and M. Zabka, "Moduli spaces of Morse functions for persistence," *Journal of Applied and Computational Topology*, vol. 4, pp. 353–385, 2020.
- [12] L. Kanari, A. Garin, and K. Hess, "From trees to barcodes and back again: theoretical and statistical perspectives," arXiv preprint arXiv:2010.11620, 2020.
- [13] E. Gasparovic, E. Munch, S. Oudot, K. Turner, B. Wang, and Y. Wang, "Intrinsic interleaving distance for merge trees," *arXiv:1908.00063*, 2019.
- [14] L. Yan, Y. Wang, E. Munch, E. Gasparovic, and B. Wang, "A structural average of labeled merge trees for uncertainty visualization," *IEEE Transactions on Visualization and Computer Graphics*, vol. 26, no. 1, pp. 832–842, 2020.
- [15] R. Sridharamurthy, T. B. Masood, A. Kamakshidasan, and V. Natarajan, "Edit distance between merge trees," *IEEE Transactions on Visualization and Computer Graphics*, vol. 26, no. 1, pp. 1518–1531, 2020.
- [16] J. Milnor, *Morse Theory*. New Jersey, NY, USA: Princeton University Press, 1963.
- [17] H. Edelsbrunner, D. Letscher, and A. J. Zomorodian, "Topological persistence and simplification," *Discrete & Computational Geometry*, vol. 28, pp. 511–533, 2002.
- [18] G. Carlsson, A. J. Zomorodian, A. Collins, and L. J. Guibas, "Persistence barcodes for shapes," *Proceedings of the Eurographics/ACM SIGGRAPH Symposium on Geometry Processing*, pp. 124–135, 2004.
- [19] H. Carr, J. Snoeyink, and U. Axen, "Computing contour trees in all dimensions," *Computational Geometry Theory and Applications*, vol. 24, no. 2, pp. 75–94, 2003.
- [20] G. Reeb, "Sur les points singuliers d'une forme de pfaff complètement intégrable ou d'une fonction numérique (on the singular points of a complete integral pfaff form or of a numerical function)," *Comptes rendus de l'Académie des Sciences Paris*, vol. 222, pp. 847–849, 1946.
- [21] G. Singh, F. Mémoli, and G. Carlsson, "Topological methods for the analysis of high dimensional data sets and 3D object recognition," in *Eurographics Symposium on Point-Based Graphics*, 2007, pp. 91–100.
- [22] H. Edelsbrunner, J. Harer, and A. J. Zomorodian, "Hierarchical Morse-Smale complexes for piecewise linear 2-manifolds," *Discrete and Computational Geometry*, vol. 30, no. 87-107, 2003.
- [23] C. D. Correa, P. Lindstrom, and P.-T. Bremer, "Topological spines: A structure-preserving visual representation of scalar fields," *IEEE Transactions on Visualization and Computer Graphics*, vol. 17, no. 12, pp. 1842–1851, 2011.
- [24] D. M. Thomas and V. Natarajan, "Detecting symmetry in scalar fields using augmented extremum graphs," *IEEE Transactions on Visualization and Computer Graphics*, vol. 19, no. 12, pp. 2663–2672, 2013.
- [25] H. Saikia, H. P. Seidel, and T. Weinkauf, "Extended branch decomposition graphs: Structural comparison of scalar data," *Computer Graphics Forum*, vol. 33, no. 3, pp. 41–50, 2014.
- [26] V. Narayanan, D. M. Thomas, and V. Natarajan, "Distance between extremum graphs," *IEEE Pacific Visualization Symposium*, pp. 263–270, 2015.
- [27] D. Laney, P.-T. Bremer, A. Mascarenhas, P. Miller, and V. Pascucci, "Understanding the structure of the turbulent mixing layer in hydrodynamic instabilities," *IEEE Transactions on Visualization and Computer Graphics*, vol. 13, no. 1, pp. 1053–1060, 2007.
- [28] J. Reininghaus, J. Kasten, T. Weinkauf, and I. Hotz, "Efficient computation of combinatorial feature flow fields," *IEEE Transactions on Visualization and Computer Graphics*, vol. 18, no. 9, pp. 1563–1573, 2012.
- [29] J. Reininghaus, N. Kotava, D. Günther, J. Kasten, H. Hagen, and I. Hotz, "A scale space based persistence measure for critical points in 2d scalar fields," *IEEE Transactions on Visualization and Computer Graphics*, vol. 17, no. 12, pp. 2045–2052, 2011.
- [30] H. Saikia and T. Weinkauf, "Global feature tracking and similarity estimation in time-dependent scalar fields," *Computer Graphics Forum*, vol. 36, no. 3, pp. 1–11, 2017.
- [31] M. Soler, M. Plainchault, B. Conche, and J. Tierny, "Lifted wasserstein matcher for fast and robust topology tracking," *arXiv:1808.05870*, 2018.
- [32] B. Wang, P. Rosen, P. Skraba, H. Bhatia, and V. Pascucci, "Visualizing robustness of critical points for 2D time-varying vector fields," *Computer Graphics Forum (CGF, Proceedings of EuroVis)*, vol. 32, no. 3pt2, pp. 221–230, 2013.
- [33] B. Wang and I. Hotz, "Robustness for 2d symmetric tensor field topology," in *Modeling Analysis and Visualization of Anisotropy*, ser. Mathematics and Visualization, I. Hotz, E. Özarslan, and T. Schultz, Eds., Springer, 2017.
- [34] J. Jankowai, B. Wang, and I. Hotz, "Robust extraction and simplification of 2D tensor field topology," *Computer Graphics Forum (CGF, Proceedings of EuroVis)*, vol. 38, no. 3, pp. 337–349, 2019.
- [35] D. Cohen-Steiner, H. Edelsbrunner, and J. Harer, "Stability of persistence diagrams," *Discrete & Computational Geometry*, vol. 37, pp. 103–120, 2007.
- [36] H. Edelsbrunner and J. Harer, "Persistent homology - a survey," *Contemporary Mathematics*, vol. 453, pp. 257–282, 2008.
- [37] D. Cohen-Steiner, H. Edelsbrunner, J. Harer, and Y. Mileyko, "Lipschitz functions have l_p -stable persistence," *Foundations of Computational Mathematics*, vol. 10, no. 2, pp. 127–139, 2010.
- [38] K. Beketayev, D. Yeliussizov, D. Morozov, G. Weber, and B. Hamann, "Measuring the distance between merge trees," *Topological Methods in Data Analysis and Visualization III: Theory, Algorithms, and Applications, Mathematics and Visualization*, pp. 151–166, 2014.
- [39] T. Le and M. Yamada, "Persistence fisher kernel: A Riemannian manifold kernel for persistence diagrams," *Advances in Neural Information Processing Systems*, vol. 31, pp. 10 028–10 039, 2018.
- [40] J. Reininghaus, S. Huber, U. Bauer, and R. Kwitt, "A stable multi-scale kernel for topological machine learning," *Proceedings of the IEEE Conference on Computer Vision and Pattern Recognition*, pp. 4741–4748, 2015.
- [41] D. Morozov, K. Beketayev, and G. Weber, "Interleaving distance between merge trees," *Proceedings of Topology-Based Methods in Visualization (TopoInVis)*, 2013.
- [42] U. Bauer, X. Ge, and Y. Wang, "Measuring distance between reeb graphs," *Proceedings of the 30th Annual Symposium on Computational Geometry*, pp. 464–474, 2014.
- [43] M. Carrière and S. Oudot, "Local equivalence and intrinsic metrics between Reeb graphs," in *Proceedings of the 33rd International Symposium on Computational Geometry*, ser. Leibniz International Proceedings in Informatics (LIPIcs), B. Aronov and M. J. Katz, Eds., vol. 77. Dagstuhl, Germany: Schloss Dagstuhl–Leibniz-Zentrum fuer Informatik, 2017, pp. 25:1–25:15.
- [44] U. Bauer, C. Landi, and F. Memoli, "The Reeb graph edit distance is universal," *Proceedings of the 36th International Symposium on Computational Geometry*, 2020.
- [45] F. Mémoli, Z. Smith, and Z. Wan, "Gromov-Hausdorff distances on p -metric spaces and ultrametric spaces," *arXiv: 1912.00564*, 2019.
- [46] T. Dey, D. Shi, and Y. Wang, "Comparing graphs via persistence distortion," *Proceedings of the 31st Annual Symposium on Computational Geometry*, pp. 491–506, 2015.
- [47] Z. Smith, S. Chowdhury, and F. Memoli, "Hierarchical representations of network data with optimal distortion bounds," *50th Asilomar Conference on Signals, Systems and Comroxiuters*, 2016.
- [48] G. Carlsson and F. Mémoli, "Characterization, stability and convergence of hierarchical clustering methods," *Journal of Machine Learning Research*, vol. 11, pp. 1425–1470, 2010.
- [49] G. Cardona, A. Mir, F. Rosselló, L. Rotger, and D. Sánchez, "Cophenetic metrics for phylogenetic trees, after Sokal and Rohlf," *BMC Bioinformatics*, vol. 14, no. 1, p. 3, 2013.
- [50] F. Chazal, D. Cohen-Steiner, M. Glisse, L. J. Guibas, and S. Y. Oudot, "Proximity of persistence modules and their diagrams," in *Proceedings of the 25th Annual Symposium on Computational Geometry*. New York, NY, USA: ACM, 2009, pp. 237–246.
- [51] F. Chazal, V. de Silva, M. Glisse, and S. Oudot, *The Structure and Stability of Persistence Modules*. Springer International Publishing, 2016.
- [52] E. Munch and A. Stefanou, "The ℓ^∞ -cophenetic metric for phylogenetic trees as an interleaving distance," in *Research in Data Science*, ser. Association for Women in Mathematics Series. Springer International Publishing, 2019, pp. 109–127.
- [53] E. F. Touli and Y. Wang, "FPT-algorithms for computing Gromov-Hausdorff and interleaving distances between trees," *Proceedings of the 27th Annual European Symposium on Algorithms*, pp. 83:1–83:14, 2019.
- [54] V. de Silva, E. Munch, and A. Patel, "Categorified Reeb graphs," *Discrete and Computational Geometry*, pp. 1–53, 2016.
- [55] J. Curry, "Sheaves, cosheaves and applications," Ph.D. dissertation, University of Pennsylvania, 2014.
- [56] E. Munch and B. Wang, "Convergence between categorical representations of Reeb space and mapper," *International Symposium on Computational Geometry (SOCG)*, 2016.

- [57] P. Bubenik, V. de Silva, and J. Scott, "Metrics for generalized persistence modules," *Foundations of Computational Mathematics*, vol. 15, no. 6, pp. 1501–1531, 2014.
- [58] V. de Silva, E. Munch, and A. Stefanou, "Theory of interleavings on categories with a flow," *Theory and Applications of Categories*, vol. 33, no. 21, pp. 583–607, 2018.
- [59] K. Zhang, "A constrained edit distance between unordered labeled trees," *Algorithmica*, vol. 15, pp. 205–222, 1996.
- [60] I. Baeza Rojo and T. Günther, "Vector field topology of time-dependent flows in a steady reference frame," *IEEE Transactions on Visualization and Computer Graphics*, vol. 26, no. 1, pp. 280–290, 2020.
- [61] S. Popinet, "Free computational fluid dynamics," *ClusterWorld*, vol. 2, no. 6, 2004. [Online]. Available: <http://gfs.sf.net/>
- [62] S. Gerber, P.-T. Bremer, V. Pascucci, and R. Whitaker, "Visual exploration of high dimensional scalar functions," *IEEE Transactions on Visualization and Computer Graphics*, vol. 16, pp. 1271–1280, 2010.
- [63] P.-T. Bremer, D. Maljovec, A. Saha, B. Wang, J. Gaffney, B. K. Spears, and V. Pascucci, "ND2AV: N-dimensional data analysis and visualization – analysis for the national ignition campaign," *Computing and Visualization in Science*, vol. 17, no. 1, pp. 1–18, 2015.
- [64] T. Athawale, D. Maljovec, L. Yan, C. R. Johnson, V. Pascucci, and B. Wang, "Uncertainty visualization of 2D Morse complex ensembles using statistical summary maps," *IEEE Transactions on Visualization and Computer Graphics*, 2020.
- [65] T. Günther, M. Gross, and H. Theisel, "Generic objective vortices for flow visualization," *ACM Transactions on Graphics*, vol. 36, no. 4, pp. 141:1–141:11, 2017.
- [66] I. Hoteit, X. Luo, M. Bocquet, A. Köhl, and B. Ait-El-Fquih, "Data assimilation in oceanography: Current status and new directions," in *New Frontiers in Operational Oceanography*, E. P. Chassignet, A. Pascual, J. Tintoré, and J. Verron, Eds. GODAE OceanView, 2018.
- [67] P. Zhan, G. Krokos, D. Guo, and I. Hoteit, "Three-dimensional signature of the Red Sea eddies and eddy-induced transport," *Geophysical Research Letters*, vol. 46, no. 4, pp. 2167–2177, 2019.
- [68] P. Zhan, A. C. Subramanian, F. Yao, and I. Hoteit, "Eddies in the red sea: A statistical and dynamical study," *Journal of Geophysical Research*, vol. 119, no. 6, pp. 3909–3925, 2014.
- [69] M. Kerber, D. Morozov, and A. Nigmetov, "Geometry helps to compare persistence diagrams," *Journal of Experimental Algorithms*, vol. 22, no. 1.4, 2017.
- [70] H. Edelsbrunner, J. Harer, and A. Zomorodian, "Hierarchical Morse complexes for piecewise linear 2-manifolds," in *Proceedings of the 17th Annual Symposium on Computational Geometry*, Medford, MA, USA, 2001, pp. 70–79.

Lin Yan is a PhD student in the Scientific Computing and Imaging (SCI) Institute, University of Utah. Her research interests include topological data analysis and visualization. Her recent work includes statistical analysis and uncertainty visualization of topological descriptors.

Talha Bin Masood is a Postdoctoral Fellow at Linköping University in Sweden. He received his Ph.D. in Computer Science from the Indian Institute of Science, Bangalore. His research interests include scientific visualization, computational geometry, computational topology, and their applications to various scientific domains.

Farhan Rasheed is PhD student at Linköping University in Sweden. He graduated from Heidelberg University with a degree in Scientific Computing. His research interests includes scientific visualization, topological data analysis, machine learning, and medical image computing.

Ingrid Hotz is currently a Professor in Scientific Visualization at the Linköping University in Sweden. She received her Ph.D. degree from the Computer Science Department at the University of Kaiserslautern, Germany. Her research interests lie in data analysis and scientific visualization, ranging from basic research questions to effective solutions to visualization problems in applications.

Bei Wang is an Assistant Professor at the School of Computing and a faculty member at the SCI Institute, University of Utah. She received her Ph.D. in Computer Science from Duke University. Her research interests include topological data analysis, data visualization, computational topology, computational geometry, machine learning, and data mining.